

Differential effects of climate change on average and peak demand for heating and cooling across the contiguous United States

Yash Amonkar^{1,2}, James Doss-Gollin³, David J. Farnham⁴, Vijay Modi⁵, and Upmanu Lall^{1,2}

¹*Columbia Water Center, Columbia University*

²*Department of Earth and Environmental Engineering, Columbia University*

³*Department of Civil and Environmental Engineering, Rice University*

⁴*ClimateAI, San Francisco, CA, USA*

⁵*Department of Mechanical Engineering, Columbia University*

Abstract

While most electricity systems are designed to handle peak demand during summer months, pathways to deep decarbonization generally electrify building heating, thus increasing electricity demand during winter. A key question is how climate variability and change will affect peak heating and cooling demand in an electrified future. We conduct a spatially explicit analysis of trends in temperature-based proxies of electricity demand over the past 70 years. Average annual demand for heating (cooling) decreases (increases) over most of the contiguous US. However, while climate change drives robust increases in peak cooling demand, trends in peak heating demand are generally smaller and less robust. Because the distribution of temperature exhibits a long left tail, severe cold snaps dominate the extremes of thermal demand. As building heating electrifies, system operators must account for these events to ensure reliability.

1 Extreme weather events pose an operational risk to infrastructure systems and the humans
2 who depend on them, and are a major cause of power outages and energy price spikes across
3 the United States [1–3]. Hot (cold) temperatures create a demand for cooling (heating), which
4 in turn drive demand for energy. For example, Winter Storm Uri, which caused cascading fail-
5 ures through interconnected and interdependent infrastructure systems as well as loss of human
6 life in Texas in 2021, caused not only supply-side failures of the energy system [4] but also by
7 unanticipated surges in demand for heating [2]. Similarly in August 2020, an extreme heat wave
8 in California caused surging demand for cooling, leading the grid operator to institute rolling
9 blackouts [5].

10 This problem is not limited to the electricity sector. Severe winter weather in New England
11 can lead to scarcity-driven spikes in wholesale prices of electricity and natural gas [3]. At present,
12 peak electric load events across the contiguous United States (CONUS) occur during the summer
13 months and when high temperatures lead to demand for electricity to power air-conditioning. A
14 large fraction of energy demand for heating during the winter is met by gas or oil furnaces [6].
15 However, modeled pathways to deep decarbonization typically require electrification of sectors
16 including building heating [7], which may lead to peak demands for electricity during winter cold
17 spells [8]. Because winter temperatures are typically farther from a thermal comfort level than
18 summer temperatures, electrification of space-heating will change the seasonality of electricity
19 demand, with large portions of the United States projected to become winter peaking systems
20 [8, 9]. Thus, a key question is how climate variability and change will affect peak demands for
21 heating and cooling in an electrified future.

22 Theory and climate models offer important insights on this question. In general, anthro-
23 pogenic climate change drives robust increases in surface temperatures globally [10]. If this were
24 to lead to a shift in the distribution of temperatures without a change in the variability, then de-
25 mand for heating would decrease and demand for cooling would increase. However, warming
26 trends are accompanied by changes in the severity and duration of extreme weather events such
27 as heat waves [11], which are particularly important to understand in order to maintain a reliable
28 power grid and provide space cooling to alleviate dangerous level of heat within urban settings
29 [12]. Overall, shifts in the average temperature are better understood than shifts in the extremes,
30 particularly cold extremes. While broad scientific consensus points to increasing frequency and
31 magnitude of heat waves [13], long-term changes in frequency of mid-latitude winter extreme
32 temperatures or cold snaps are uncertain potentially driven by Arctic Amplification and remain
33 an active area of research [14, 15].

34 In this paper, we present a retrospective analysis of trends in heating and cooling demand
35 using temperature-based proxies of energy demand for the last 72 years (1950–2021) over the
36 CONUS using climate reanalysis data [16]. We quantify both changes to annual average energy
37 demand and to annual maximum (peak) energy demands, which are key design parameters for
38 energy and electricity systems [17, 18]. Moreover, peak load supply is generally more expensive
39 compared to ordinary supply plants and contributes disproportionately to consumer costs. We
40 focus on understanding historical trends and their system reliability implications for near-term
41 operations and investment, given that in the long term deeply uncertain technological and socio-
42 economic factors will drive system performance [19]. We identify a north-south divide in the
43 emergent patterns of the heating, cooling, and total thermal demand trends, especially for the
44 ratio of average to peak demands and the relative importance of the peak cooling and peak heating
45 demand. To aggregate findings to decision-relevant scales, we estimate trends for major electric

46 grid systems and present findings for Florida and the Midcontinent Independent System Operator
 47 (MISO), which serve as the archetypes of the grid in the north and south.

48 1 Trends in annual mean inferred thermal demand

49 Mean heating and cooling demand contribute to the total demand for energy and have direct
 50 implications for carbon emissions and energy economics. A first question is how the average
 51 annual demand for heating and cooling has changed over the past 70 years. To answer this
 52 question, we consider the average annual demand for cooling and heating inferred from hourly
 53 temperature data from the ERA-5 reanalysis dataset [16]. Specifically, we define the inferred
 54 demand for heating and cooling , at each grid cell and for each hour, as the difference between
 55 the hourly temperature and a threshold temperature of 65°F; see Methods for additional details.
 56 These can be interpreted as the number of degrees a building must be cooled or heated to reach
 57 a thermal comfort level. We also define the total thermal demand as the sum of the cooling and
 58 heating demand.

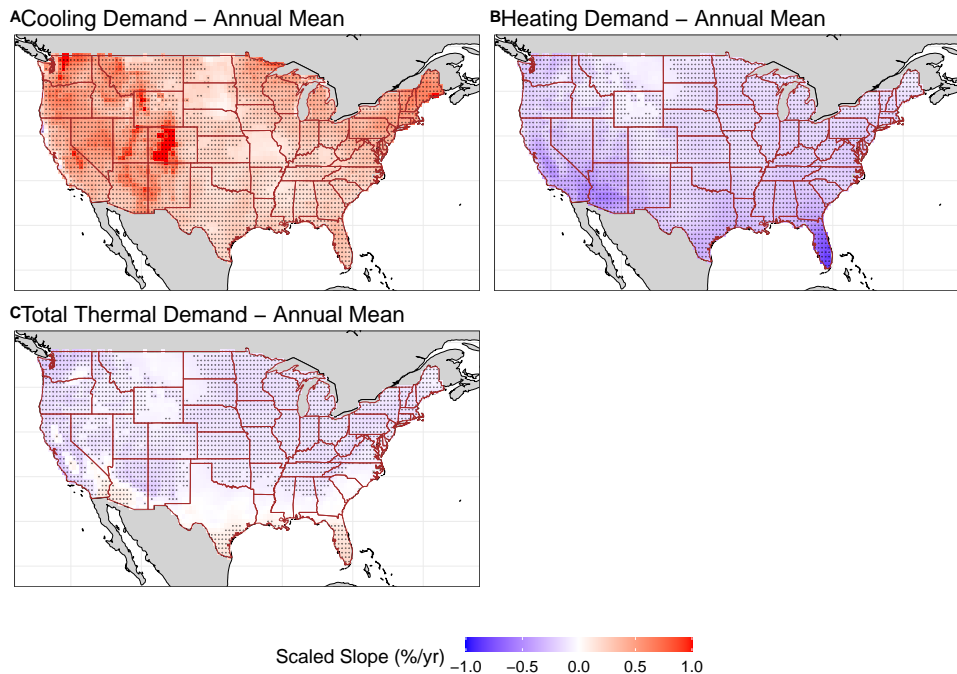


Figure 1: Demand for cooling (heating) is increasing (decreasing) across the contiguous United States (CONUS), with net decreases in all but the hottest climates. Trends (see Methods for details) in annual mean demand for (A) cooling, (B) heating, and (C) total thermal demand across the CONUS at each grid cell ($0.5^\circ \times 0.5^\circ$ lat-lon) across the CONUS from ERA5 [16]. The shaded colors denote the estimated trend per year (%/yr). The dotted regions are locations where the trend in the mean inferred demand is statistically significant at the 5% level.

59 Figure 1 shows robust increases in annual demand for cooling and robust decreases in de-
 60 mand for heating across the CONUS. This is consistent with first-order expectations from climate

change, which is expected to increase the temperature and length of summers and to shorten the length and severity of winters [20]. The dark red regions, especially in central Colorado, show the largest increases in demand for cooling, with the trend being greater than 1%/yr, and the dark blue regions, especially in the southern Florida, show the largest decreases in demand for heating, with the trend being below -1%/yr. This is also consistent with expectations about regional climate change in Southern Florida [21] and in Colorado with higher elevations generally recording higher warming rates [22] and could be driven by changes in the snow telemetry stations [23].

These competing shifts lead to differential trends in total thermal demand by region. Across most of CONUS, total thermal demand shows robust negative trends because winters are longer and farther from a thermal comfort level than summers. However, in southern states where summers are particularly long and hot, the increased demand for cooling outweighs the decreased demand for heating; these trends are significant in some parts of Florida, Arizona, Texas, and Southern California. Field significance tests (see Methods) reject the hypothesis of no trend for all three demand types.

While analysis at the scale of reanalysis grid cells is useful for understanding the spatial patterns of trends, it is not directly relevant to the operation of the electric grid. Electric Grids, Independent System Operators, and Regional Transmission Operators are socio-political entities over which grid planning and operations are coordinated. Such entities have boundaries of operation and serve dedicated population centers and regions. As such, ensuring adequate supply and reliability of electricity is a key concern for these entities. Moreover, electric grids are designed for the peak load and increasing electric generation capacity is capital intensive and requires analysis of forecasts and trends in projected demand [17]. To answer this question, we aggregate the thermal trends over space, weighting each grid cell by its 2020 population [24].

Figure 2 shows the aggregated trends in the total thermal demand for the Florida Electric Grid and the Midcontinent Independent Systems Operator (MISO), which are representative of the hot and cold regions of the CONUS, respectively. The Florida grid (Figure 2 (A)) covers most of the state of Florida, with the exception of the panhandle and is the southernmost sub-grid within the CONUS. Like other southern regions, average inferred cooling demand is greater than the average inferred heating demand, and so the net trend is towards increasing total thermal demand (figure 2C). Florida is the only grid entity within the CONUS (see Methods for a list of all entities examined) where the total thermal load has a statistically significant increasing trend.

An opposite trend is apparent for the region served by MISO (fig. 2B). Because of its northern location, MISO has an inferred heating demand much larger than the inferred cooling demand (fig. 2D). Consequently, the increasing background temperature leads the decreasing heating demand to dominate the total thermal demand, resulting in a net decrease in total thermal demand. This trend is representative for other grid entities serving northern regions (figure S6–S8). This indicates that a scenario with total electrification of space heating would see decreasing demand on average across the Northern CONUS.

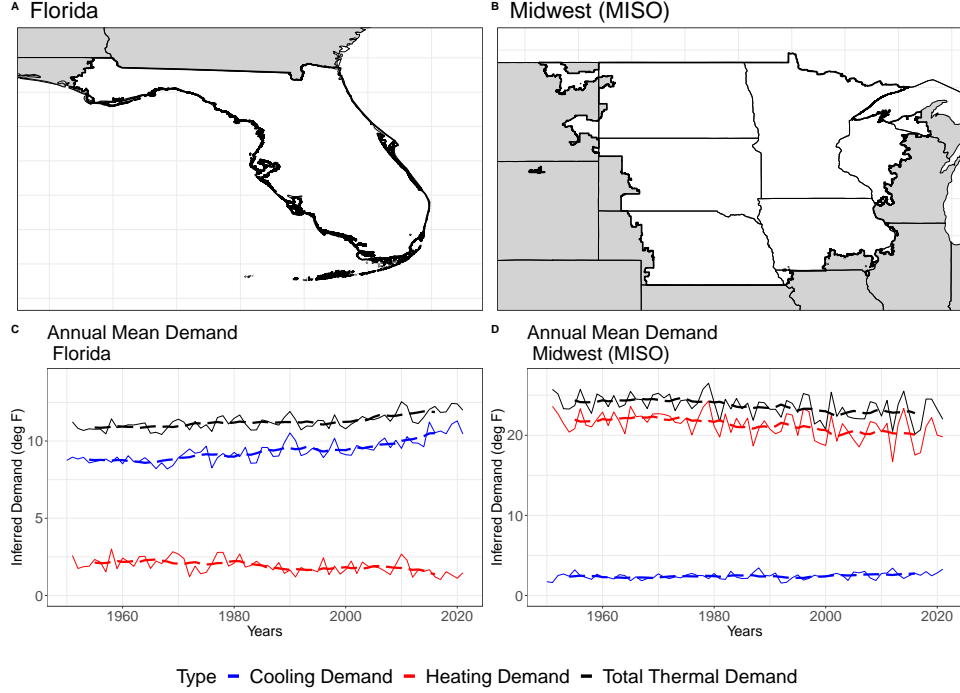


Figure 2: While demand for heating (cooling) is decreasing (increasing) across the contiguous United States (CONUS), the net effect is a decrease in total thermal demand in cold regions and a net increase in total thermal demand in hot regions. Two archetypes of grid operators serving hot (A-Florida) and cold (B-MISO) regions are shown. (C): annual mean inferred demand in terms of degrees Fahrenheit for Florida. (D): annual mean inferred demand in terms of degrees Fahrenheit for MISO. Red lines show decreasing demand for heating, blue lines show increasing demand for cooling, and black lines show increasing (decreasing) total thermal demand for Florida (MISO). The dashed lines denote a 10-yr moving average.

99 2 Trends in annual peak inferred thermal demand

100 Although the annual mean thermal demand is a useful metric for understanding the long-term
 101 trends in thermal demand, an equally important metric is the peak thermal demand. Peak de-
 102 signs are important for ensuring reliability of the electrical [17] and other energy systems [3]
 103. Peak electrical demands are already projected to increase as other sectors of the economy (e.g.,
 104 transportation) electrify [25]. To answer this question, we examine the time series of the maxi-
 105 mum (instead of mean considered in the previous section) 72-hour inferred thermal demand from
 106 the same datasets. The effect of extreme temperature events on energy demand is a function of
 107 the event's length and intensity with short term spikes interrupting plant operations and spik-
 108 ing prices while long duration events also causing breakdown of critical infrastructure services.
 109 Similar analysis was also carried out for peak inferred demand events for durations ranging from
 110 6 hours to 336 hours (14 days).

111 Consistent with a background increase in temperature, increases (decreases) in peak demand
 112 for cooling (heating) are observed across large swaths of CONUS (figure 3A-B). Across large
 113 swaths of the CONUS, the peak inferred cooling demand intensity (duration 72 hours) has in-

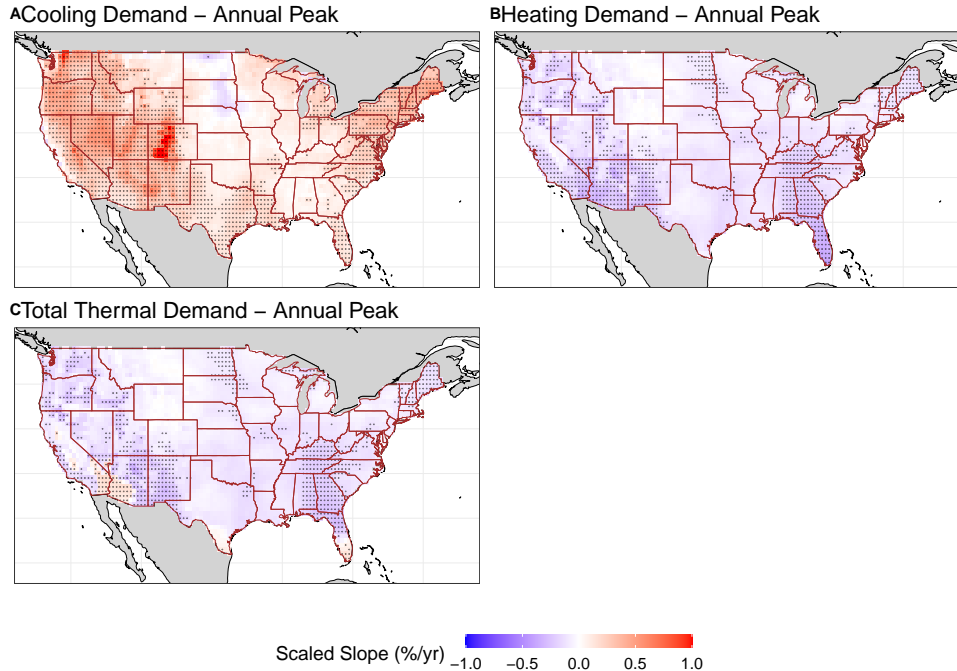


Figure 3: Trends in the intensity of peak inferred cooling, heating, and total thermal demand across the CONUS are more variable than the trends in the mean demands but are most coherent for cooling demand in the Western and Northeastern portions of the CONUS, where cooling demands have been increasing. Trends in the intensity of peak inferred demand events of duration 72 hours for (A) cooling demand, (B) heating demand, and (C) total thermal demand at the reanalysis grid-cell level ($0.5^\circ \times 0.5^\circ$ lat-lon) across the CONUS. The shaded colors denote the estimated trend per year (%/yr). The dotted regions are locations where the trend in demand is statistically significant at the 5% level. Peak events correspond to the annual maximum events (see Methods for further details).

114 creased, whereas the peak inferred heating demand intensity has decreased. The peak thermal load also shows decreasing trends throughout the CONUS, except for the southernmost regions (Figure 3 C). Furthermore, we find no systematic shift or change in the seasonality and day-of-year occurrence of peak inferred heating and cooling demand events. Field significance tests were also run and the hypothesis of no trend was rejected for all three demand types.

119 The peak inferred cooling demand intensity for events with a duration of 72 hours (Figure 3
120 A) shows increasing trends across most of the CONUS. The median trend is 0.16%/yr, whereas the
121 range extends from -0.25%/yr to 1.77%/yr. The estimated slope of the trend is largest in central
122 Colorado, with an annual increase greater than 1%/yr. Almost all of the western United States,
123 New England, New York, Florida, Louisiana, Pennsylvania and large portions of Texas, Virginia,
124 and North Carolina have increasing cooling demand intensity trends that are statistically signif-
125 icant. This is in contrast to interior regions of the Midwest and the Plains, which exhibit smaller
126 trends, and the Dakotas, which even exhibit a small decreasing trend in the peak cooling demand.
127 Similar trends, including the large increases within Colorado and decreases within the Dakotas,
128 are seen in peak events when other event durations are considered (Figure S2).

129 Almost the entire CONUS has had decreasing trends in the peak inferred heating demand
 130 intensity for events with a duration of 72 hours (Figure 3 (B)). The median trend is -0.1 %/yr,
 131 with the range being (-0.41, 0.03) %/yr. Unlike the peak cooling demand intensity, there are no
 132 areas with large increases and the trends are significant mostly in Southern California and the
 133 southwest and southeast portions of the CONUS, which are regions where the heating demand
 134 during the winter is low and does not dominate grid operations. The nature of the trends in peak
 135 heating event intensity is fairly constant across multiple durations (Figure S3).

136 Trends in peak inferred thermal load intensity for events for a 72 hour duration (Figure 3
 137 (C)) have a median and range of -0.1 %/yr and (-0.37, 0.20) %/yr, respectively. The statistically
 138 significant trends are concentrated in the southern parts of the Western United States, from Ap-
 139 palachia to Florida and in the upper Northeast of the country. Almost all of the CONUS shows
 140 an overall decrease in the peak thermal load intensity driven by the decrease in the peak heating
 141 demand intensity (Figure 3 (B)), which is typically larger than the peak cooling demand intensity.
 142 Exceptions are the southernmost parts of Florida, Texas, Arizona, and California, where there is
 143 an increase driven by the peak cooling demand intensity that exceeds the peak heating demand
 144 intensity. Trends for other event durations have similar spatial patterns (Figure S4).

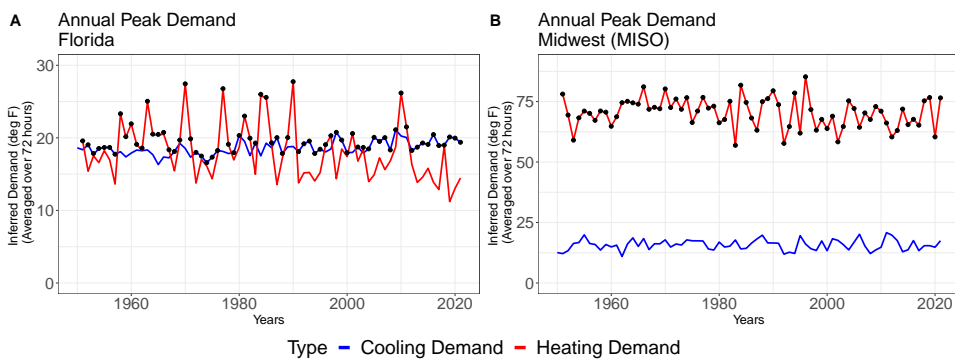


Figure 4: The magnitude of inter-annual variability in the intensity of peak heating events is much larger than that of peak cooling events, as shown for both Florida and the Midwest (MISO). Peak Inferred Demand Intensity for events of duration 72 hours in population adjusted degrees Fahrenheit averaged over 72 hours for (A) Florida, and (B) MISO. The red and blue colors correspond to heating and cooling demand, respectively. The black dots correspond to peak events for the total thermal load.

145 The secular trends that were present in the mean heating, cooling, and total thermal demand
 146 (Figure 2) are less prominent in the peak events for both Florida and MISO (Figure 4). Instead,
 147 the peak heating demand is marked by substantial inter-annual and decadal variability (Figure
 148 4). Florida has an increasing peak cooling demand trend and a recent decline in the peak heating
 149 demand intensity. Such trends are not evident for MISO. Similar plots of the peak inferred demand
 150 intensity for other grid sub-regions are attached in the supplement (Figure S9 - S11).

151 The peak event intensity for total thermal load for Florida (Figure 4 (A)), is typically asso-
 152 ciated with the peak cooling demand, but dramatically higher peak heating demands occur in
 153 several years corresponding to cold outbreaks. The peak cooling demand events dominate post
 154 2010. Thus, for grid operators in the Southern United States, a challenge is the variability in the
 155 peak heating demand, which far exceeds the variability in the peak cooling demand. For MISO

(Figure 4 (B)), the peak total thermal demand events are exclusively the peak heating demands, exhibiting increasing inter-annual variability post 1980. Consequently, a seasonal prediction for the winter to anticipate either a high or a low heating demand peak is crucial for timing system maintenance and upgrades and allocating adequate capacity. For example, the planned outages for plant maintenance coincided during the Texas freeze of Feb 2021 [2, 4], in anticipation of a future summer peak.

3 Trends in Thermal Load Factors

An additional measure of grid operation viability is the load factor [26], which is a measure of the efficiency of electricity usage. The load factor is defined as the ratio of average load to peak load over a specific time interval. It measures the average utilization of the installed capacity of electric infrastructure systems. While the overall grid economics are determined by numerous factors, including governmental policies, the peak loads and load factors are indicators of the overall supply-side economics of the grid.

The utilization of installed system capacity is a key criterion in energy economics and infrastructure management [27]. Infrastructure utilization is often measured by a load factor defined as the annual mean demand divided by the peak demand for the same year. In this section, we look at only how climate affects utilization rates. Demand fluctuations for other reasons for example, population and efficiency of technology, are amplified by thermal load considerations. The installed capacity should be determined by the expected peak demand. In the current context, we consider the peak thermal demand as the design criteria, assuming that it is the dominant additive determinant of the peak load on the system, and consider the utilization factor through the ratio of the mean thermal load to the peak thermal load.

Large portions of the southern United States show an increasing trend in thermal load factors, though trends are statistically significant only in the southernmost regions. The trends in the infrastructure utilization rates (load factors) for thermal demand are shown in Figure 5. The median and range of the trends are 0.01 %/yr and (-0.17, 0.42) %/yr, respectively. For example, within the Florida grid sub-region (Figure 6 (A)), thermal load factors show an increasing trend with large decadal variability, mirroring our earlier observation of the peak heating trend. A silver lining is that while the peak thermal load in Florida (Figure 4 (A)) is increasing, the mean thermal load is increasing faster, translating into higher load factors or greater utilization of the needed capacity. A much milder trend (decreasing mainly in the 1950s) is evident for MISO (Figure 6 (B)). There is high inter-annual variability in the load factor for both MISO and Florida, largely due to dramatic year-to-year changes in the peak heating load, re-emphasizing the importance of accurate seasonal forecasts for the peak heating load or winter cold outbreaks.

The northern parts of the CONUS and parts of the Western mountain regions have decreasing load factor trends (significant in parts of California, and the Great Lakes region) (Figure 5). The mean thermal load is decreasing faster than the peak in these areas. Few areas, including parts of Southern California and Arizona, are driven by different dynamics, where the decreasing load factors are driven by slower increases in the mean thermal demand than the peak. These trends are similar for other event durations (Figure S5). Further, plots of the load factors for other grid sub-regions are attached in the supplement (Figure S12 - S14).

Similarly, these predominant trends in Florida and MISO are also visualized in load duration

Thermal Load Factor

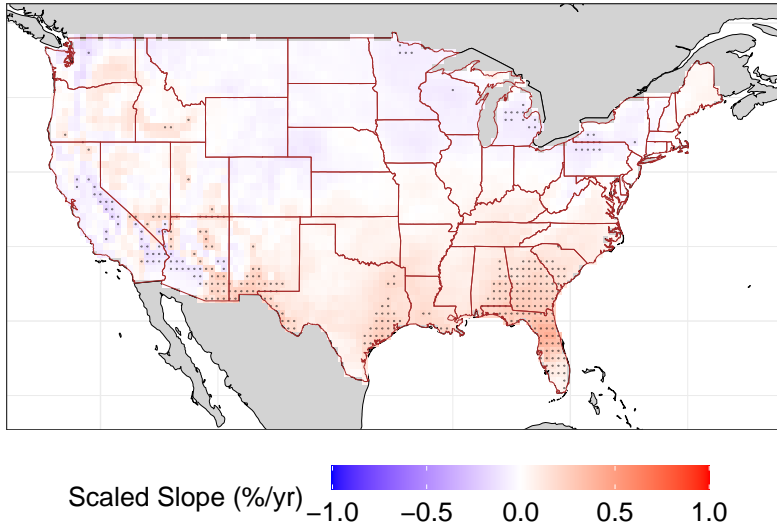


Figure 5: Trends in the thermal load factors across the CONUS are heterogeneous, with a spatially coherent pattern of positive trends in the Southeastern US. Trends in load factors for total thermal demand at the grid-cell level ($0.5^\circ \times 0.5^\circ$ lat-lon) across the CONUS. The peak event demand intensity is computed for events with a duration of 72 hours. The shaded colors denote the estimated trend per year (%/yr). The dotted regions are locations where the trend in the load factors is statistically significant at the 5% level.

198 curves [28] that represent the relative frequency of demand exceedance (Figure S15). The load
199 duration curves for other grid sub-regions are attached in the supplement (Figure S16 - S18).
200 Overall, the ongoing process of electrification of space-heating is poised to increase the actual
201 electric peak load across large parts of the country [8]. Once completed, however, the infra-
202 structure built to meet the peak load may see lower utilization rates in the northern parts of the
203 United States driven by decreases in the mean heating demand (Figure 1), which are larger than
204 the decreases in peak demand (Figure 3). Lower infrastructure utilization rates are associated
205 with higher average operating costs that are then passed on to consumers.

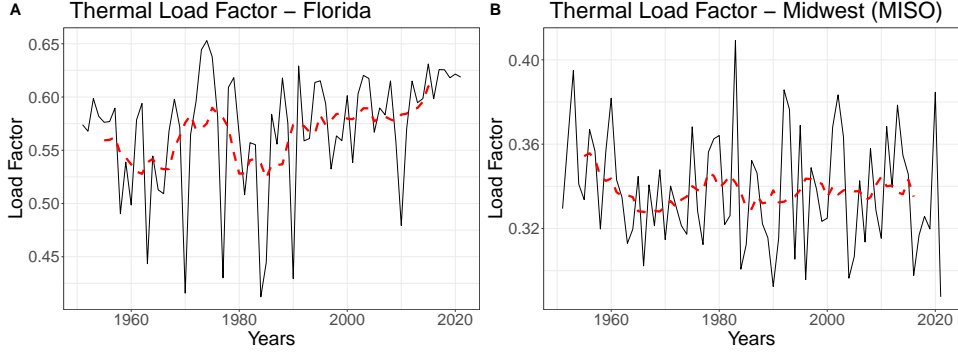


Figure 6: Trends in the annual thermal load factors are contrasting for Florida (increasing) and Midwest (MISO; slightly decreasing), though both regions exhibit substantial inter-annual and inter-decadal variability. Annual Load factors for total thermal load for (A) Florida, (B) MISO. The load factors are defined as the annual mean load divided by the annual peak load. Peak demand load is computed for events of a duration of 72 hours. The dashed red line denotes a 10-yr moving average.

206 4 Conclusions

207 As expected under a global warming regime, there have been significant changes in the ther-
 208 mal loads experienced by electric grid operators across the CONUS. Overall, the average winter
 209 heating demand is decreasing, whereas the average summer cooling demand is increasing. The
 210 dynamics are less consistent in the case of peak load events, where the peak heating load is rela-
 211 tively unchanged across large swaths of the CONUS while the peak cooling load is increasing in
 212 the population dense regions.

213 There are divergent trends in the hypothetical capacity utilization over the historical record
 214 that impact regional energy economics. The average heating demand is decreasing faster than the
 215 peak heating demand, leading to decreasing load factors in the northern regions of the CONUS,
 216 where the heating load dominates the grid. In the southernmost regions of the CONUS, where
 217 cooling loads dominate, the average cooling demand is increasing faster than the peak cooling
 218 demand, leading to increasing load factors. If these divergent trends in capacity utilization are
 219 manifest, due to widespread electrification of heating, and continue into the future, they will
 220 effectively result in progressively increasing costs needed to maintain reliable power systems in
 221 northern regions of the CONUS and decreasing costs needed to maintain reliable power systems
 222 in southernmost areas of the CONUS. In fact, this analysis is a precursor to evaluating results
 223 from climate model simulations of future climate conditions.

224 Lastly, our results show that peak heating demand during winter is characterized by very high
 225 inter-annual variability. This variability is difficult to manage without procuring massive reserve
 226 capacity during winter and/or improving our ability to predict such winter peak events with
 227 sufficient lead times to adjust normal system operations, such as by postponing regular seasonal
 228 maintenance. We recently witnessed some of the significant electric grid problems that can occur
 229 due to poor anticipation of a severe cold outbreak in Texas in 2021 during winter storm Uri [2].

230 **5 Data and Methods**

231 **5.1 Temperature**

232 The 2-meter surface temperature data are taken from ERA-5 reanalysis data product [16]. The
233 spatial grid size of the data is set at 0.5° lat \times 0.5° lon and contains 3267 grid points within the
234 contiguous United States (Figure S19 (A)). The data are at an hourly time-step and span 72 years
235 (1950-2021).

236 **5.2 Population**

237 The population data are taken from the Gridded Population of the World, Version 4 (GPWv4)
238 [24]. The population for the year 2020 is used in this study. The data files were produced as global
239 rasters at 30 arc-second (1 km at the equator) resolution but aggregated to the spatial resolution
240 of the reanalysis dataset.

241 **5.3 Electric Grid Sub-Regions**

242 The CONUS is divided into three major grids - Western Interconnection, Eastern Interconnec-
243 tion, and Electric Reliability Council of Texas. These three interconnections are further divided
244 into Regional Transmission Organizations, Independent System Operators, and additional sub-
245 regions. We use the Environmental Protection Agency's (EPA) Emissions & Generation Resource
246 Integrated Database (eGRID) maps for the shape-files of the various grid sub-regions [29]. The
247 eGRID sub-regions are regional entities of EPA's Clean Air Markets Division and roughly cor-
248 respond to the grid sub-regions. We make the following changes in the shape-files to have the
249 eGRID sub-regions better reflect the grid subregions. The eGRID sub-regions of New York City,
250 Long Island, and New York State are merged to better reflect the New York Independent Sys-
251 tem Operator (NYISO), which covers the entire state of New York. The spatial extent of the grid
252 sub-regions is shown in Figure S19 (B). The list of the grid entities analyzed in this study are
253 (A) - Arizona/New Mexico, (B) - CAISO, (C) - ERCOT, (D) - Florida, (E) - Wisconsin (Rural), (F)
254 - Midwest (MISO), (G) - ISO New England, (H) - Northwest, (I) - NYISO, (J) - PJM (West), (K) -
255 Michigan, (L) - PJM (East), (M) - Colorado, (N) - Kansas, (O) - Oklahoma, (P) - Arkansas/Louisiana,
256 (Q) - Missouri, (R) - Southeast, (S) - Tennessee Valley, (T) - Carolinas (Figure S19 (B)).

257 **5.4 Inferred heating, cooling and total thermal demand at the local level**

258 The local inferred demand is computed for each grid-cell where the ERA-5 temperature data are
259 available. The residential heating and cooling demand are functions of the temperature deviation
260 from a temperature most suited for human comfort [8]. The total thermal demand is defined as
261 the sum of both the heating and cooling demand (total temperature dependent inferred demand).

262 Using $65^{\circ}F$ ($18.33^{\circ}C$, $291.5^{\circ}K$) as the ambient temperature threshold, the deviation of ob-
263 served temperature from this threshold is taken as the proxy inferred heating and cooling de-
264 mand. Our overall conclusions are not sensitive to the ambient temperature threshold. Different
265 thresholds (e.g., $68^{\circ}F$) also lead to similar macro level trends. The ERA-5 data are available at an
266 hourly resolution and the inferred heating and cooling demand was computed as

$$HD_{i,t} = \max(65 - T_{i,t}, 0) \quad (1)$$

$$CD_{i,t} = \max(T_{i,t} - 65, 0) \quad (2)$$

$$TTD_{i,t} = |T_{i,t} - 65| \quad (3)$$

where, $HD_{i,t}$, $CD_{i,t}$, $TTD_{i,t}$, and $T_{i,t}$ are the inferred heating demand, inferred cooling demand, inferred total thermal demand, and observed temperature at hour t and location i .

5.5 Population distribution weighted inferred demand at the regional level

All the ERA-5 temperature locations (grid-cells) within the electric grid sub-region of interest are identified and the inferred thermal demand is computed for each grid-cell using the method described above. The grid-cell level inferred demand is then multiplied by the regional population fraction associated with that location (grid-cell) and summed across all locations (grid-cells) within the electric grid sub-region of interest. The population weighted inferred heating, cooling, and total thermal demand are defined as,

$$HD_t = \sum_{i=1}^N \max(65 - T_{i,t}, 0) \times f_i$$

$$CD_t = \sum_{i=1}^N \max(T_{i,t} - 65, 0) \times f_i$$

$$TTD_t = \sum_{i=1}^N |T_{i,t} - 65| \times f_i$$

where, HD_t , CD_t , TTD_t are the population adjusted inferred heating, cooling and total thermal demand for hour t . $T_{i,t}$ is the observed temperature for location i at hour t . N is the total number of ERA-5 temperature grid-cells within the grid sub-region of interest. f_i is the population fraction associated with the grid-cell i . The 2020 population was used to assess the population fractions f_i . Thus, the trends computed are sensitive to temperature only, and not to population changing over time.

5.6 Peak Inferred Demand

We use the annual maxima of the thermal load over a particular duration (e.g., a moving window of 72 hours) as the criteria to define peak events [30]. This relates directly to the generation capacity needed for grid operations as an addition to other loads. The annual maximum peak intensity of heating, cooling or total thermal demand for an event of duration 72 hours is computed as:

$$I_y = \max_t \left(\sum_{t=m}^{m+71} ID_{t[y]} \right) \quad 1 < m < (n - 72), y = 1...k$$

288 where, I_y is the peak demand intensity for year y for events of duration 72 hours, ID_t is the
 289 inferred demand for hour t . n is the total number of hours t in year y , and k is the total number
 290 of years.

291 The annual cycle for identifying peak inferred cooling demand events is set as January-December,
 292 whereas the annual cycle for identifying peak inferred heating and total thermal demand events
 293 is set as September-August. This ensures seasonal continuity since the peak inferred heating
 294 demand events occur most frequently during the boreal winter (December-January-February).
 295 A consequence of this transformation is that peak inferred cooling demand data extends from
 296 1950-2021 (72 year), whereas the peak inferred heating and total thermal demand data spans only
 297 1951-2021 (71 years).

298 5.7 Statistical Analysis

299 5.7.1 Trend Analysis for Direction

300 The Mann-Kendall (MK) trend test is used to check for the presence of a monotonic trend in
 301 the time series data and is a non-parametric rank based test making it applicable to any data
 302 irrespective of the underlying generative probability distribution [31]. The two-sided MK test is
 303 used to check for the presence of either a monotonic increasing or decreasing trend in the data.
 304 The MK test statistic (Z_S) for a time series x_1, x_2, \dots, x_n is computed as:-

$$S = \sum_{i=1}^{n-1} \sum_{j=i+1}^n sgn(x_j - x_i)$$

305 where sgn is the sign operator taking values -1,0,1 for the negative, zero and positive values
 306 respectively.

$$Z_S = \begin{cases} \frac{S-1}{\sigma_S} & \text{if } S > 0 \\ 0 & \text{if } S = 0 \\ \frac{S+1}{\sigma_S} & \text{if } S < 0 \end{cases}$$

307 The null hypothesis of this test is rejected at significance level α if $|Z_S| > Z_{crit}$ where Z_{crit}
 308 is the value of the standard normal distribution with a probability of exceedance of $\alpha/2$. The
 309 significance level selected for this study is 5%. Refer [31] for additional details on computation of
 310 σ_S and effect of the sample size n .

311 5.7.2 Trend Analysis for Slope

312 Thiel-Sen slope (b_S), a rank based test statistic, is computed as a robust estimate of the monotonic
 313 trend. The estimate, a median of the pairwise slopes between elements of the series, is based on
 314 a non-parametric test and can be applied to all distributions. The validity of this test does not
 315 depend on the normality of the residuals and is not strongly affected by outliers, unlike ordinary
 316 least square regression [31].

317 The estimate is computed using each pair of observations in a pairwise manner, resulting in
 318 $n \times (n - 1)/2$ individual computations. For each data pair the slope between the two points is

319 computed. The median of all such values is the required slope. The significance test for the slope
320 is identical to the procedure above.

$$b_s = \text{median} \frac{(y_j - y_i)}{(x_j - x_i)} \quad \text{for all } i < j$$

321 The Mann-Kendall trend test and Thiel-Sen's slope estimation were conducted using the *trend*
322 package [32].

323 5.7.3 Field Significance Test

324 The field significance test is used to check whether the total number of tests that show a significant
325 result could have happened by chance, given that a large number of tests were conducted. The
326 null hypothesis of this test is that the fraction of grid cells exhibiting a monotonic linear trend at
327 $\alpha\%$ level of significance can be attributed to random chance and spatial correlation between the
328 grid cells [33, 34]. The test is conducted using a bootstrap that resamples the entire field by time,
329 thus addressing the potential spatial correlation in the data.

330 For each bootstrap sample, the significance test described earlier is run at all the grid points.
331 The total number of grid points that turn up significant are noted. This procedure is repeated
332 for 1000 bootstrap samples. The $(1 - \alpha)^{th}$ percentile of the number of grid points significant for
333 the 1000 bootstrapped samples is compared against the data. If the number of significant grid-
334 points in the data is greater than the $(1 - \alpha)^{th}$ percentile from the bootstrapped copies, the null
335 hypothesis of the field significance test at the $\alpha\%$ level of significance is rejected [34].

336 5.8 Data and Code Availability

337 The ERA-5 temperature data, population data-set and shapefiles can be accessed publicly. All
338 code used in this study is made publicly available in a GitHub repository and can be accessed from
339 <https://github.com/yashamonkar/CONUS-Inferred-Heating-Cooling>.

340 References

- 341 1. Smith, A. *U.S. Billion-dollar Weather and Climate Disasters, 1980 - present (NCEI Accession*
342 *0209268)* en. Last Modified: 2022-10-21. 2020. [https://www.ncei.noaa.gov/
343 access/metadata/landing-page/bin/iso?id=gov.noaa.nodc:
344 0209268](https://www.ncei.noaa.gov/access/metadata/landing-page/bin/iso?id=gov.noaa.nodc:0209268) (2022).
- 345 2. Doss-Gollin, J., Farnham, D. J., Lall, U. & Modi, V. How unprecedented was the February 2021
346 Texas cold snap? en. *Environmental Research Letters* **16**. Publisher: IOP Publishing, 064056.
347 ISSN: 1748-9326. <https://dx.doi.org/10.1088/1748-9326/ac0278> (2022)
348 (June 2021).
- 349 3. Akdemir, K. Z., Kern, J. D. & Lamontagne, J. Assessing risks for New England's whole-
350 sale electricity market from wind power losses during extreme winter storms. en. *Energy*
351 **251**, 123886. ISSN: 0360-5442. [https://www.sciencedirect.com/science/
352 article/pii/S0360544222007897](https://www.sciencedirect.com/science/article/pii/S0360544222007897) (2022) (July 2022).

- 353 4. Busby, J. W. *et al.* Cascading risks: Understanding the 2021 winter blackout in Texas. en. *Energy Research & Social Science* **77**, 102106. ISSN: 2214-6296. <https://www.sciencedirect.com/science/article/pii/S2214629621001997> (2022) (July 2021).
- 354 5. CAISO. *Final Root Cause Analysis: Mid-August 2020 Extreme Heat Wave* tech. rep. (Jan. 2021).
355 <http://www.caiso.com/Documents/Final-Root-Cause-Analysis-Mid-August-2020-Extreme-Heat-Wave.pdf> (2022).
- 356 6. Cao, X., Dai, X. & Liu, J. Building energy-consumption status worldwide and the state-of-the-
357 art technologies for zero-energy buildings during the past decade. en. *Energy and Buildings*
358 **128**, 198–213. ISSN: 0378-7788. <https://www.sciencedirect.com/science/article/pii/S0378778816305783> (2022) (Sept. 2016).
- 359 7. Steinberg, D. *et al. Electrification and Decarbonization: Exploring U.S. Energy Use and Green-
360 house Gas Emissions in Scenarios with Widespread Electrification and Power Sector Decar-
361 bonization* English. Tech. rep. NREL/TP-6A20-68214 (National Renewable Energy Lab. (NREL),
362 Golden, CO (United States), July 2017). <https://www.osti.gov/biblio/1372620/> (2022).
- 363 8. Waite, M. & Modi, V. Electricity Load Implications of Space Heating Decarbonization Path-
364 ways. en. *Joule* **4**, 376–394. ISSN: 2542-4351. <https://www.sciencedirect.com/science/article/pii/S2542435119305781> (2022) (Feb. 2020).
- 365 9. Mai, T. T. *et al. Electrification Futures Study: Scenarios of Electric Technology Adoption and
366 Power Consumption for the United States* English. Tech. rep. NREL/TP-6A20-71500 (National
367 Renewable Energy Lab. (NREL), Golden, CO (United States), June 2018). <https://www.osti.gov/biblio/1459351> (2022).
- 368 10. Rohde, R. *et al.* A New Estimate of the Average Earth Surface Land Temperature Spanning
369 1753 to 2011. en. *Geoinformatics & Geostatistics: An Overview* **2013**. Publisher: SciTechnol.
370 https://www.scitechnol.com/new-estimate-of-the-average-earth-surface-land-temperature-spanning-to-1eCc.php?article_id=450 (2022) (Jan. 2014).
- 371 11. Seneviratne, S. I., Donat, M. G., Mueller, B. & Alexander, L. V. No pause in the increase of
372 hot temperature extremes. en. *Nature Climate Change* **4**. Number: 3 Publisher: Nature Pub-
373 lishing Group, 161–163. ISSN: 1758-6798. <https://www.nature.com/articles/nclimate2145> (2022) (Mar. 2014).
- 374 12. Sailor, D. J. Risks of summertime extreme thermal conditions in buildings as a result of cli-
375 mate change and exacerbation of urban heat islands. en. *Building and Environment* **78**, 81–88.
376 ISSN: 0360-1323. <https://www.sciencedirect.com/science/article/pii/S0360132314001085> (2023) (Aug. 2014).
- 377 13. Shukla, P. R. *et al. Climate Change and Land: An Ipcc Special Report on Climate Change, De-
378 sertification, Land Degradation, Sustainable Land Management, Food Security, and Greenhouse
379 Gas Fluxes in Terrestrial Ecosystems* (2019).
- 380 14. Cohen, J. *et al.* Recent Arctic amplification and extreme mid-latitude weather. en. *Nature
381 Geoscience* **7**. Number: 9 Publisher: Nature Publishing Group, 627–637. ISSN: 1752-0908.
382 <https://www.nature.com/articles/ngeo2234> (2023) (Sept. 2014).

- 394 15. Barnes, E. A. Revisiting the evidence linking Arctic amplification to extreme weather in mid-
395 latitudes. en. *Geophysical Research Letters* **40**. _eprint: <https://onlinelibrary.wiley.com/doi/pdf/10.1002/grl.50>
396 4734–4739. ISSN: 1944-8007. <https://onlinelibrary.wiley.com/doi/abs/10.1002/grl.50880> (2023) (2013).
- 398 16. Hersbach, H. *et al.* The ERA5 global reanalysis. en. *Quarterly Journal of the Royal Meteorological Society* **146**. _eprint: <https://rmets.onlinelibrary.wiley.com/doi/pdf/10.1002/qj.3803>,
399 1999–2049. ISSN: 1477-870X. <https://rmets.onlinelibrary.wiley.com/doi/abs/10.1002/qj.3803> (2021) (2020).
- 402 17. Kirschen, D. S. & Strbac, G. *Fundamentals of Power System Economics* en. Google-Books-ID:
403 I9hhDwAAQBAJ. ISBN: 978-1-119-21324-6 (John Wiley & Sons, Sept. 2018).
- 404 18. ERCOT. *2022 ERCOT System Planning: Long-Term Hourly Peak Demand and Energy Forecast*
405 tech. rep. (Jan. 2022). <https://www.ercot.com/files/docs/2022/02/24/2022LTLFReport.pdf> (2022).
- 407 19. Mathy, S., Criqui, P., Knoop, K., Fischedick, M. & Samadi, S. Uncertainty management and the
408 dynamic adjustment of deep decarbonization pathways. *Climate Policy* **16**. Publisher: Taylor
409 & Francis _eprint: <https://doi.org/10.1080/14693062.2016.1179618>, S47–S62. ISSN: 1469-3062.
410 <https://doi.org/10.1080/14693062.2016.1179618> (2023) (June 2016).
- 411 20. Pachauri, R. K. *et al. Climate Change 2014: Synthesis Report. Contribution of Working Groups
412 I, II and III to the Fifth Assessment Report of the Intergovernmental Panel on Climate Change* (eds
413 Pachauri, R. K. & Meyer, L.) Pages: 151 Publication Title: EPIC3Geneva, Switzerland,
414 IPCC, 151 p., pp. 151, ISBN: 978-92-9169-143-2. ISBN: 978-92-9169-143-2. <https://epic.awi.de/id/eprint/37530/> (2023) (IPCC, Geneva, Switzerland, 2014).
- 416 21. Jiang, A., Zhu, Y., Elsafty, A. & Tumeo, M. Effects of Global Climate Change on Building Energy
417 Consumption and Its Implications in Florida. *International Journal of Construction Education and Research* **14**. Publisher: Routledge _eprint: <https://doi.org/10.1080/15578771.2017.1280104>,
418 22–45. ISSN: 1557-8771. <https://doi.org/10.1080/15578771.2017.1280104> (2023) (Jan. 2018).
- 421 22. Rangwala, I. & Miller, J. R. Climate change in mountains: a review of elevation-dependent
422 warming and its possible causes. en. *Climatic Change* **114**, 527–547. ISSN: 1573-1480. <https://doi.org/10.1007/s10584-012-0419-3> (2023) (Oct. 2012).
- 424 23. Ma, C., Fassnacht, S. & Kampf, S. How Temperature Sensor Change Affects Warming Trends
425 and Modeling: An Evaluation Across the State of Colorado. en. *Water Resources Research* **55**.
426 _eprint: <https://onlinelibrary.wiley.com/doi/pdf/10.1029/2019WR025921>, 9748–9764. ISSN: 1944-
427 7973. <https://onlinelibrary.wiley.com/doi/abs/10.1029/2019WR025921>
428 (2023) (2019).
- 429 24. CIESIN. *Gridded Population of the World, Version 4 (GPWv4)* tech. rep. (Socioeconomic Data
430 and Applications Center (SEDAC), 2016). <https://doi.org/10.7927/H4X63JVC>
431 (2022).
- 432 25. Pudjianto, D. *et al.* Smart control for minimizing distribution network reinforcement cost
433 due to electrification. en. *Energy Policy. Special Section: Transition Pathways to a Low Carbon
434 Economy* **52**, 76–84. ISSN: 0301-4215. <https://www.sciencedirect.com/science/article/pii/S0301421512004338> (2023) (Jan. 2013).

- 436 26. Watkins, G. P. A Third Factor in the Variation of Productivity: The Load Factor. *The American*
437 *Economic Review* 5. Publisher: American Economic Association, 753–786. ISSN: 0002-8282.
438 <https://www.jstor.org/stable/1809629> (2022) (1915).
- 439 27. Nelson, T. & Orton, F. Australia's National Electricity Market: Optimising Policy to Facilitate
440 Demand-Side Response. en. *Australian Economic Review* 49. _eprint: <https://onlinelibrary.wiley.com/doi/pdf/8462.12151>, 146–168. ISSN: 1467-8462. <https://onlinelibrary.wiley.com/doi/abs/10.1111/1467-8462.12151> (2022) (2016).
- 443 28. Poulin, A., Dostie, M., Fournier, M. & Sansregret, S. Load duration curve: A tool for technico-
444 economic analysis of energy solutions. en. *Energy and Buildings* 40, 29–35. ISSN: 0378-7788.
445 <https://www.sciencedirect.com/science/article/pii/S0378778807000278>
446 (2022) (Jan. 2008).
- 447 29. EPA. *Emissions & Generation Resource Integrated Database (eGRID)* tech. rep. (Office of At-
448 mospheric Programs, Clean Air Markets Division., Washington, DC, 2022). <https://www.epa.gov/egrid> (2022).
- 450 30. Coles, S. *An Introduction to Statistical Modeling of Extreme Values* ISBN: 978-1-84996-874-4
451 978-1-4471-3675-0. <http://link.springer.com/10.1007/978-1-4471-3675-0> (2022) (Springer, London, 2001).
- 453 31. Helsel, D. R. & Hirsch, R. M. *Statistical Methods in Water Resources* en. Google-Books-ID:
454 jao4o5X1pvgC. ISBN: 978-0-444-88528-9 (Elsevier, 1992).
- 455 32. Pohlert, T. Non-Parametric Trend Tests and Change-Point Detection. <https://CRAN.R-project.org/package=trend> (2022) (July 2017).
- 457 33. Livezey, R. E. & Chen, W. Y. Statistical Field Significance and its Determination by Monte
458 Carlo Techniques. EN. *Monthly Weather Review* 111. Publisher: American Meteorological
459 Society Section: Monthly Weather Review, 46–59. ISSN: 1520-0493, 0027-0644. <https://journals-ametsoc-org.ezproxy.cul.columbia.edu/view/journals/mwre/111/1/1520-049319831110046sfsaid20co2.xml>
460 (2021) (Jan. 1983).
- 463 34. Krishnamurthy, C. K. B., Lall, U. & Kwon, H.-H. Changing Frequency and Intensity of Rainfall
464 Extremes over India from 1951 to 2003. EN. *Journal of Climate* 22. Publisher: American
465 Meteorological Society Section: Journal of Climate, 4737–4746. ISSN: 0894-8755, 1520-0442.
466 <https://journals.ametsoc.org/view/journals/clim/22/18/2009jcli2896.1.xml> (2021) (Sept. 2009).
- 467

468 **A Supplementary Materials**

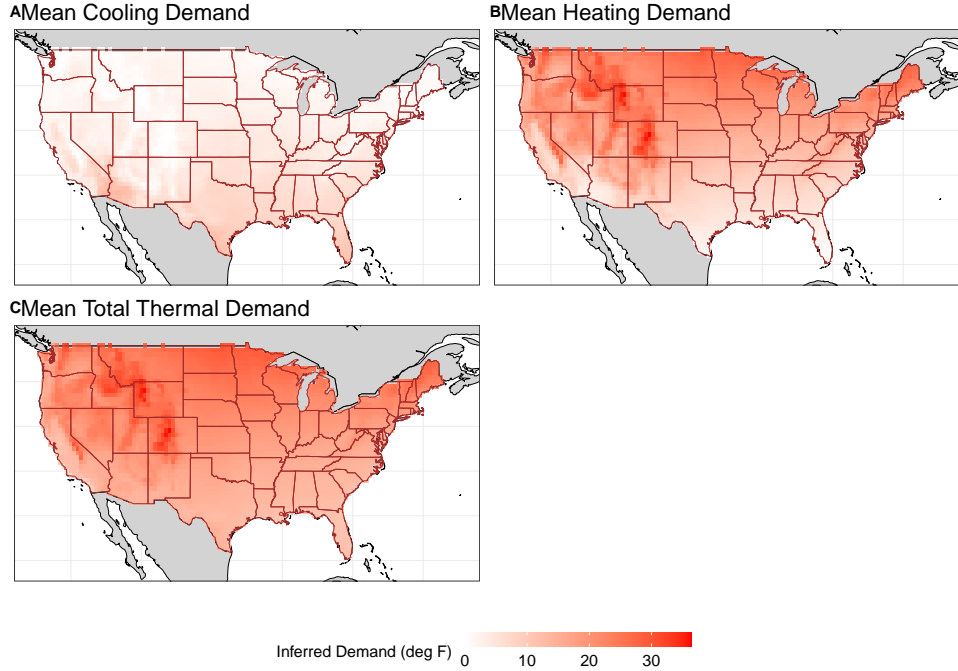


Figure S1: Mean profile for the inferred demand across the CONUS. Mean inferred (A) cooling, (B) heating, and (C) total thermal load at the reanalysis grid-cell level ($0.5^\circ \times 0.5^\circ$ lat-lon) across the CONUS. The shading denotes the inferred load in deg F.

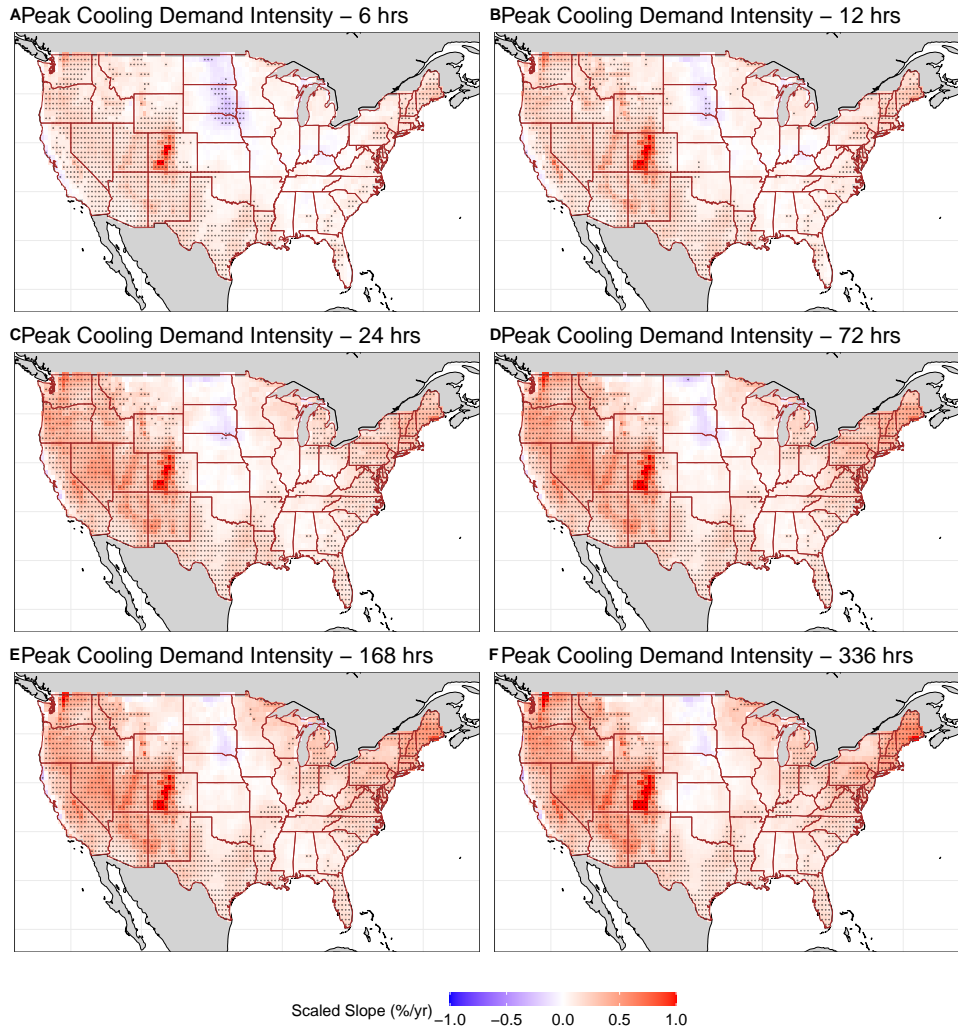


Figure S2: Trends in intensity of peak inferred cooling demand events of duration (A) 6 hours, (B) 12 hours, (C) 24 hours, (D) 72 hours, (E) 144 hours, and (F) 336 hours at the reanalysis grid-cell level ($0.5^\circ \times 0.5^\circ$ lat-lon) across the CONUS. The shaded colors denote the estimated trend per year (%/yr). The dotted regions are locations where the trend in the demand is statistically significant at the 5% level.

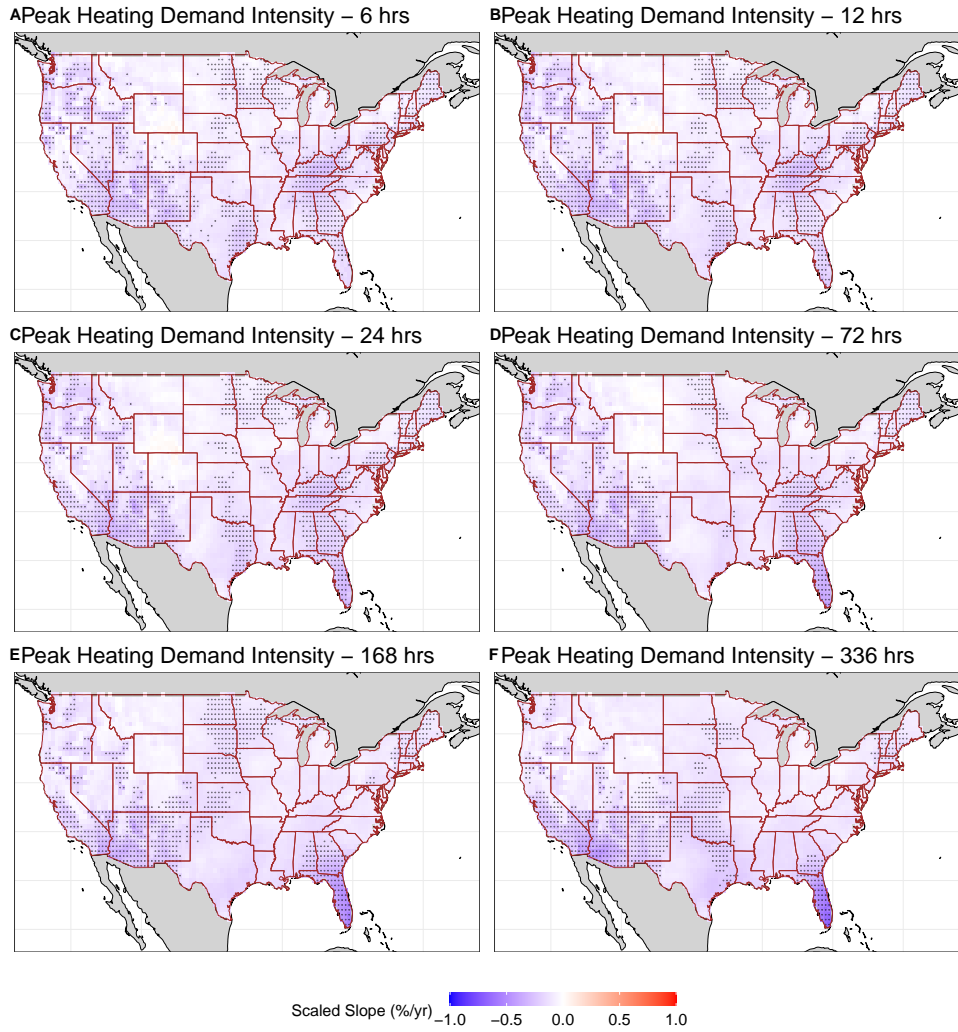


Figure S3: Trends in intensity of peak inferred heating demand events of duration (A) 6 hours, (B) 12 hours, (C) 24 hours, (D) 72 hours, (E) 144 hours, and (F) 336 hours at the reanalysis grid-cell level ($0.5^\circ \times 0.5^\circ$ lat-lon) across the CONUS. The shaded colors denote the estimated trend per year (%/yr). The dotted regions are locations where the trend in the demand is statistically significant at the 5% level.

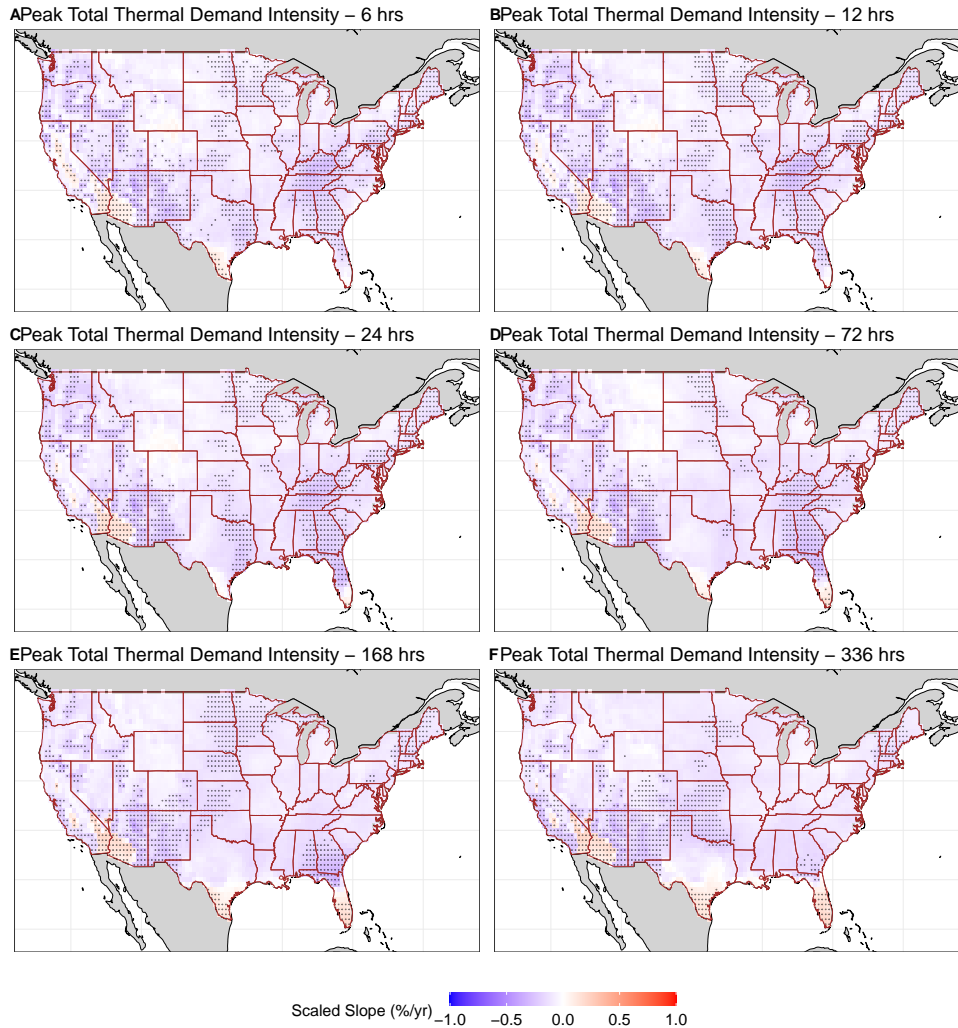


Figure S4: Trends in intensity of peak inferred total thermal demand events of duration (A) 6 hours, (B) 12 hours, (C) 24 hours, (D) 72 hours, (E) 144 hours, and (F) 336 hours at the reanalysis grid-cell level ($0.5^\circ \times 0.5^\circ$ lat-lon) across the CONUS. The shaded colors denote the estimated trend per year (%/yr). The dotted regions are locations where the trend in the demand is statistically significant at the 5% level.

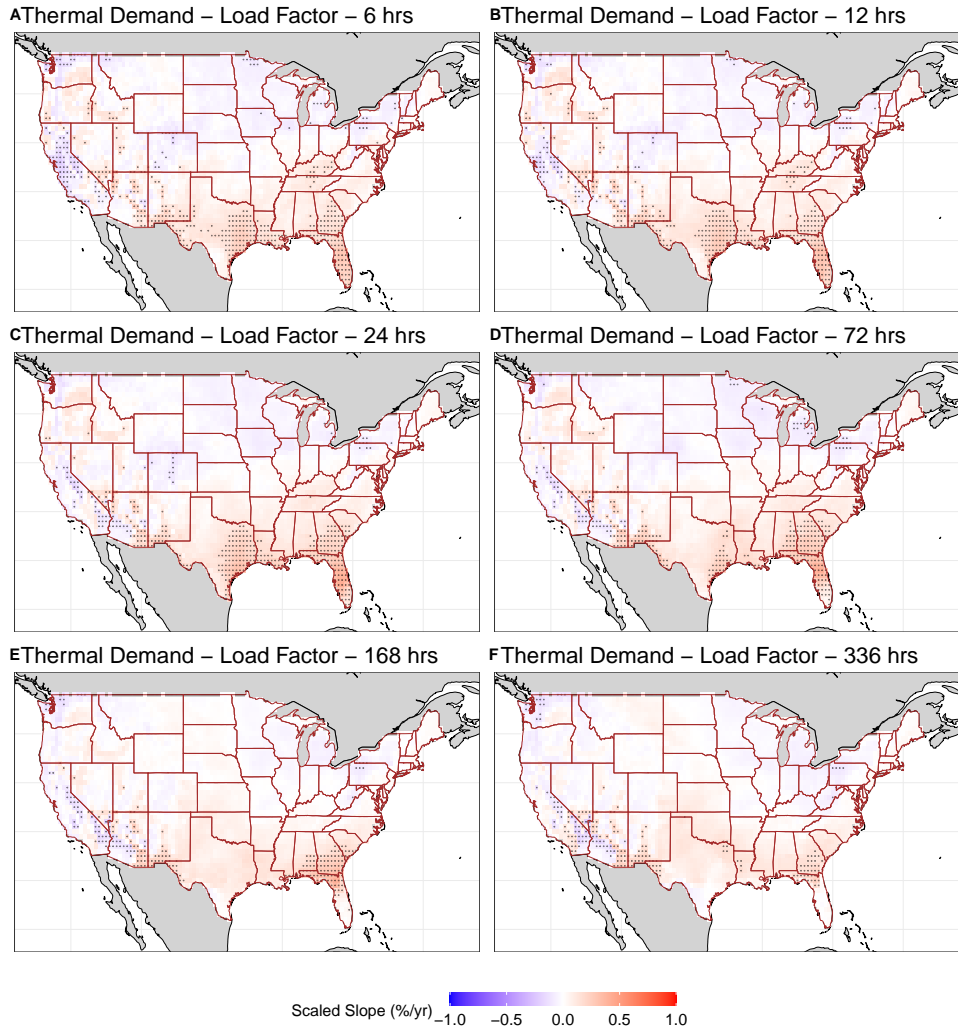


Figure S5: Trends in the infrastructure utilization rates (load factors) of total thermal demand events of duration (A) 6 hours, (B) 12 hours, (C) 24 hours, (D) 72 hours, (E) 144 hours, and (F) 336 hours at the reanalysis grid-cell level ($0.5^\circ \times 0.5^\circ$ lat-lon) across the CONUS. The shaded colors denote the estimated trend per year (%/yr). The dotted regions are locations where the trend in the demand is statistically significant at the 5% level.

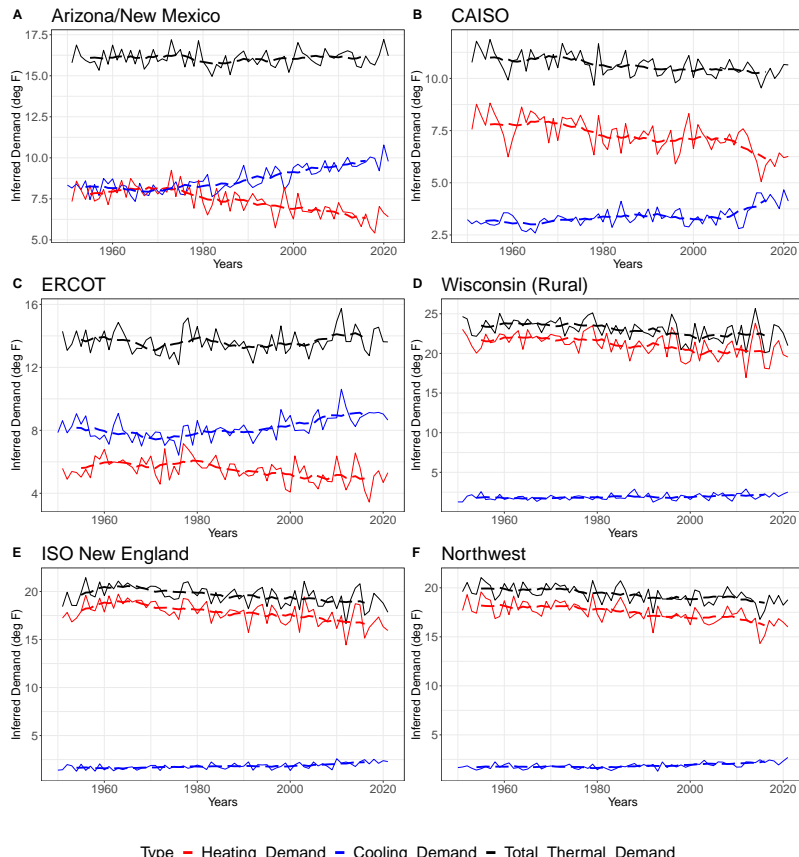


Figure S6: Annual mean inferred demand in degree Fahrenheit for different grid sub-regions. The dashed lines denote a 10-yr moving average. (A) Arizona/New Mexico, (B) CAISO, (C) ERCOT, (D) Wisconsin (Rural), (E) ISO New England, and (F) Northwest.

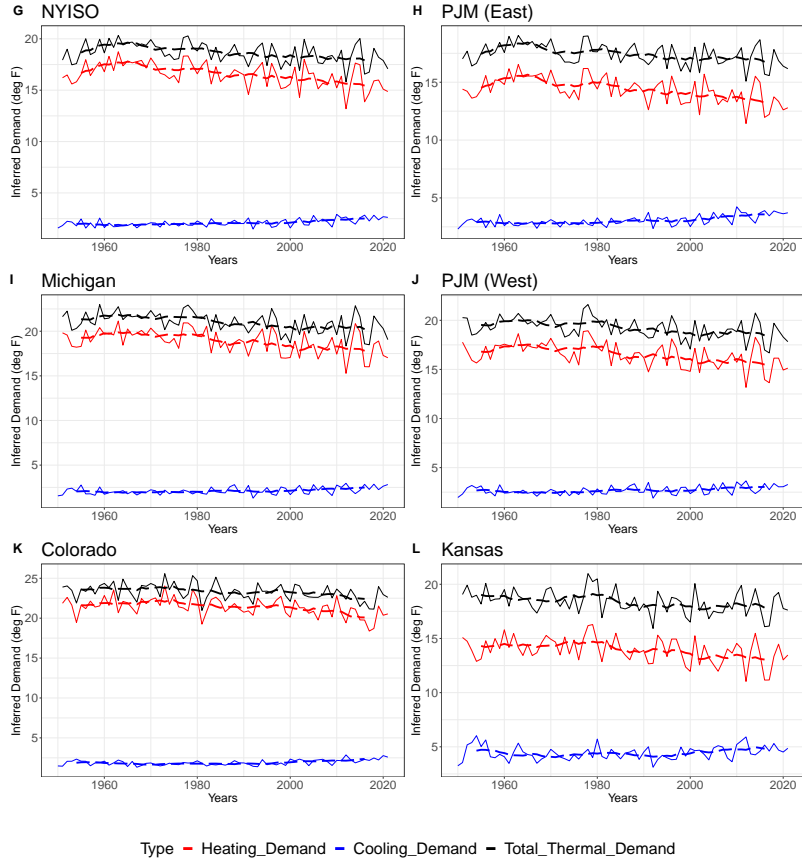


Figure S7: Annual mean inferred demand in degree Fahrenheit for different grid sub-regions. The dashed lines denote a 10-yr moving average. (G) NYISO, (H) PJM (East), (I) Michigan, (J) PJM (West), (K) Colorado, and (L) Kansas.

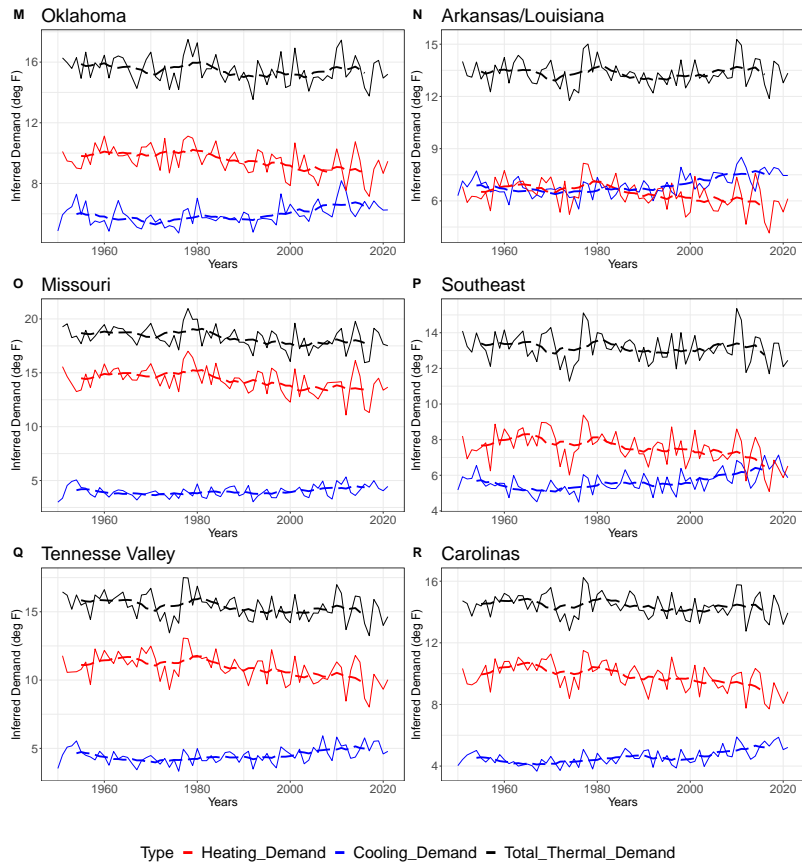


Figure S8: Annual mean inferred demand in degree Fahrenheit for different for different grid sub-regions. The dashed lines denote a 10-yr moving average. (M) Oklahoma, (N) Arkansas/Louisiana, (O) Missouri, (P) Southeast, (Q) Tennessee Valley, and (R) Carolinas.

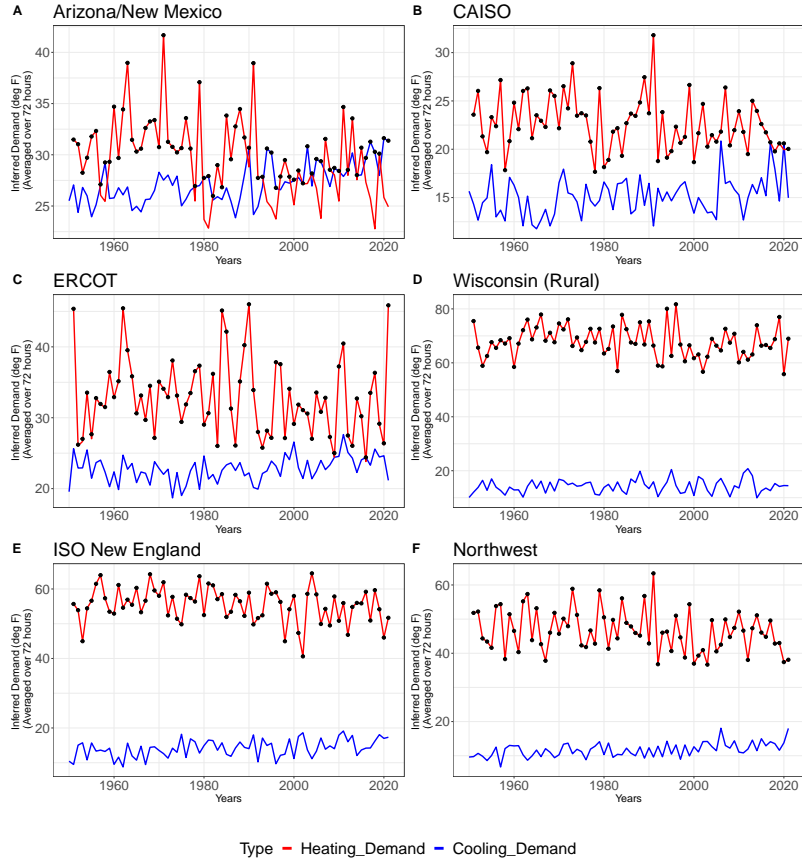


Figure S9: Peak inferred demand intensity for events of duration 72 hrs in population adjusted degrees Fahrenheit averaged over 72 hours for different grid sub-regions. The black dots correspond to peak events for the total thermal load. (A) Arizona/New Mexico, (B) CAISO, (C) ERCOT, (D) Wisconsin (Rural), (E) ISO New England, and (F) Northwest.

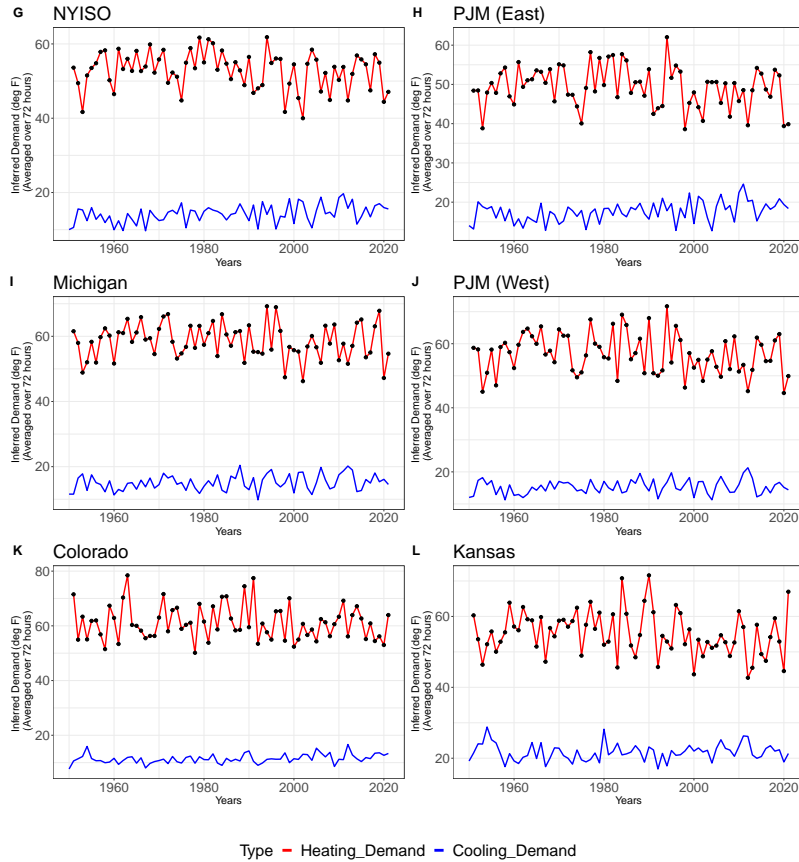


Figure S10: Peak inferred demand intensity for events of duration 72 hrs in population adjusted degrees Fahrenheit averaged over 72 hours for different grid sub-regions. The black dots correspond to peak events for the total thermal load. (G) NYISO, (H) PJM (East), (I) Michigan, (J) PJM (West), (K) Colorado, and (L) Kansas.

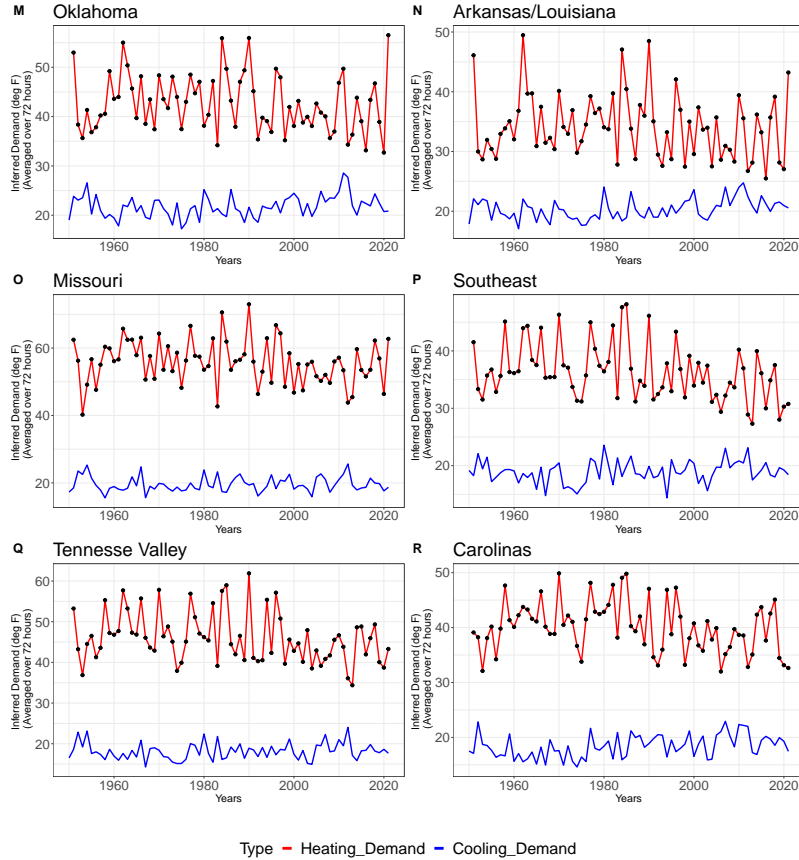


Figure S11: Peak inferred demand intensity for events of duration 72 hrs in population adjusted degrees Fahrenheit averaged over 72 hours for different grid sub-regions. The black dots correspond to peak events for the total thermal load. (M) Oklahoma, (N) Arkansas/Louisiana, (O) Missouri, (P) Southeast, (Q) Tennessee Valley, and (R) Carolinas.

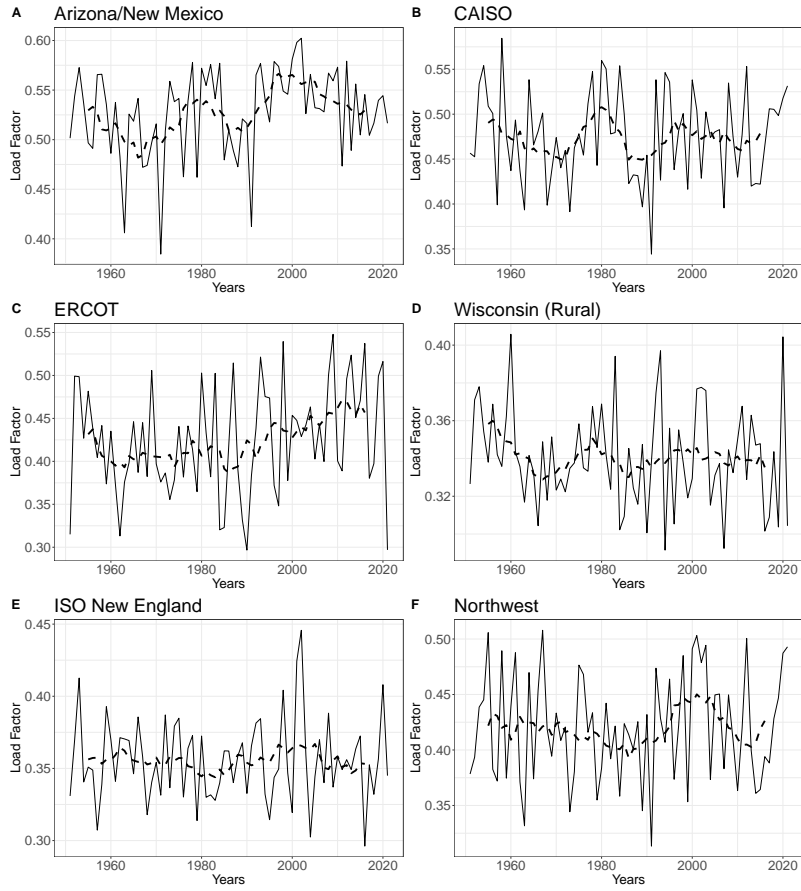


Figure S12: Annual load factors for the total thermal load for different grid sub-regions. The load factors are defined as the annual mean load divided by the annual peak load. Peak demand is computed for events of duration 72 hours. The dashed line denotes a 10-yr moving average.(A) Arizona/New Mexico, (B) CAISO, (C) ERCOT, (D) Wisconsin (Rural), (E) ISO New England, and (F) Northwest.

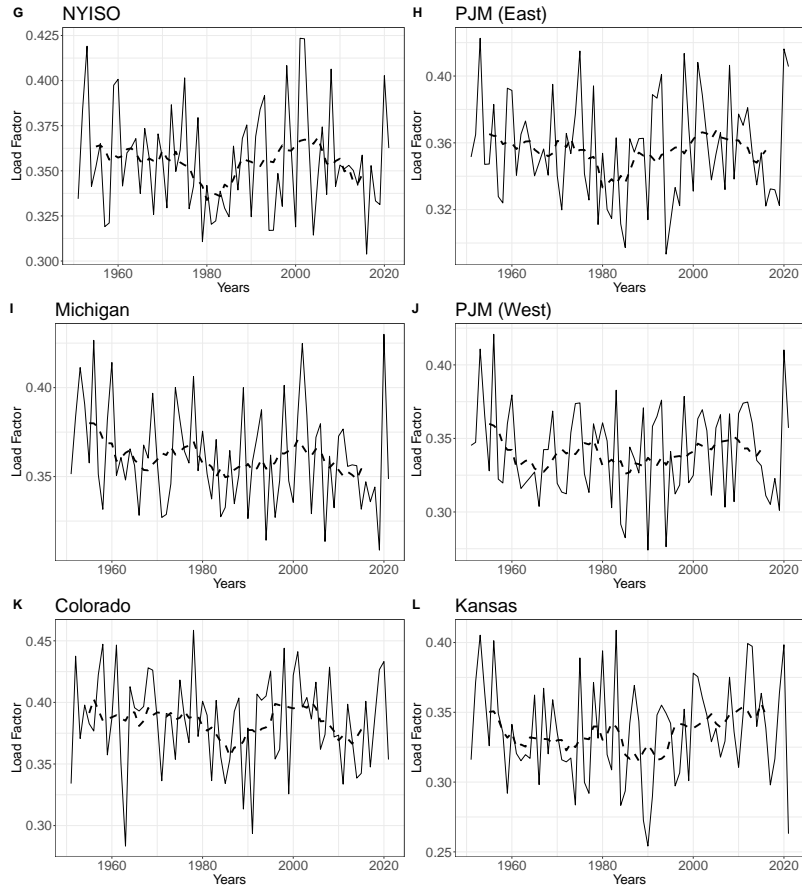


Figure S13: Annual load factors for the total thermal load for different grid sub-regions. The load factors are defined as the annual mean load divided by the annual peak load. Peak demand is computed for events of duration 72 hours. The dashed line denotes a 10-yr moving average.(G) NYISO, (H) PJM (East), (I) Michigan, (J) PJM (West), (K) Colorado, and (L) Kansas.

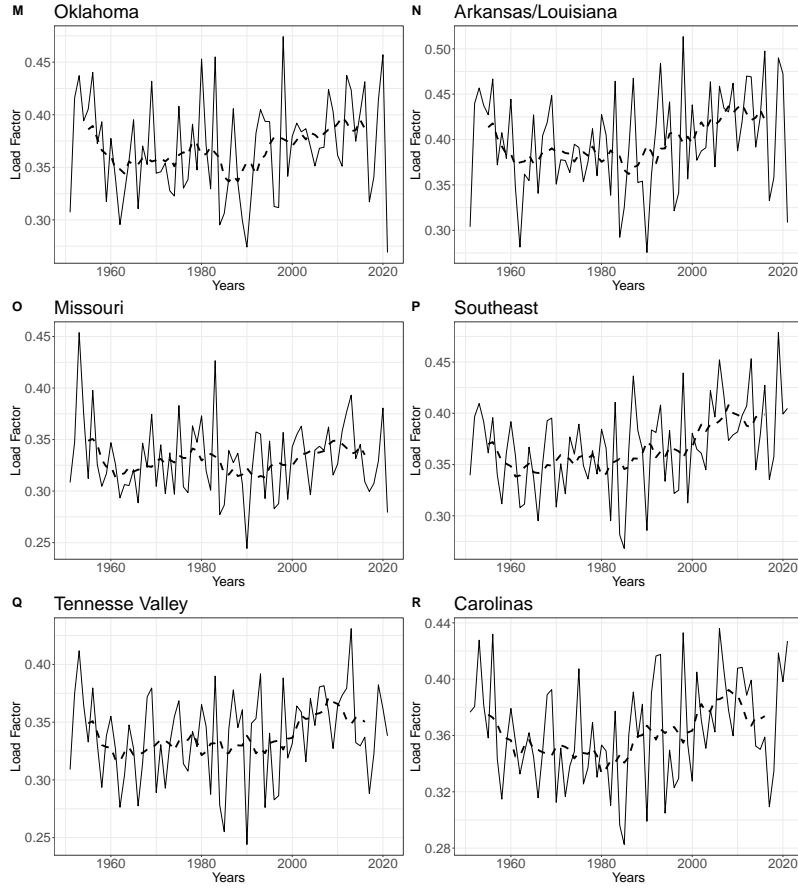


Figure S14: Annual load factors for the total thermal load for different grid sub-regions. The load factors are defined as the annual mean load divided by the annual peak load. Peak demand is computed for events of duration 72 hours. The dashed line denotes a 10-yr moving average. (M) Oklahoma, (N) Arkansas/Louisiana, (O) Missouri, (P) Southeast, (Q) Tennessee Valley, and (R) Carolinas.

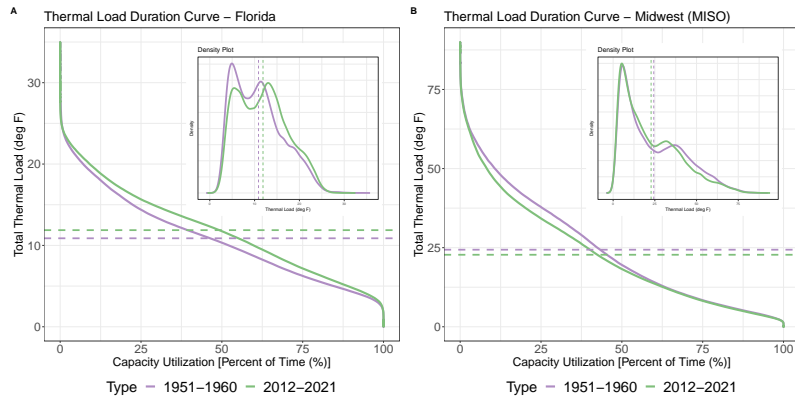


Figure S15: Thermal load duration curves for (A) Florida and (B) MISO for 1951-1960 (purple line) and 2012-2021 (green line) which correspond to the first and last 10 years of the dataset. The figure embedded inside the main figure is the probability density function (pdf) of the total thermal load for the two time periods.

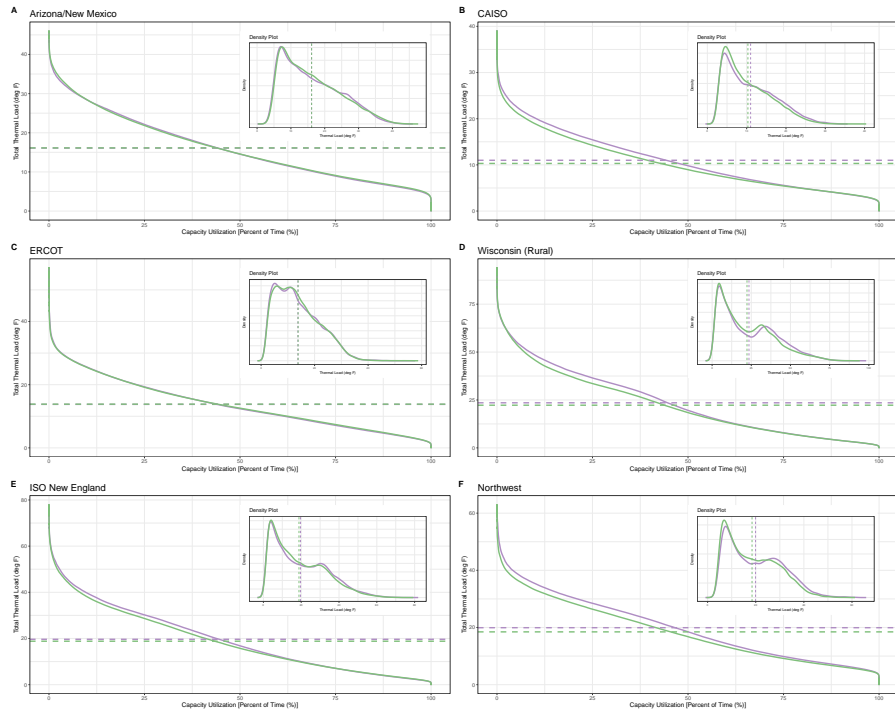


Figure S16: Load duration curves for (A) Arizona/New Mexico, (B) CAISO, (C) ERCOT, (D) Wisconsin (Rural), (E) ISO New England, and (F) Northwest for 1951-1960 (purple line) and 2012-2021 (green line) which correspond to the first and last 10 years of the dataset. The dotted lines denote their respective means. The figure inside the main figure is the probability density function (pdf) of the total thermal load for the two time periods.

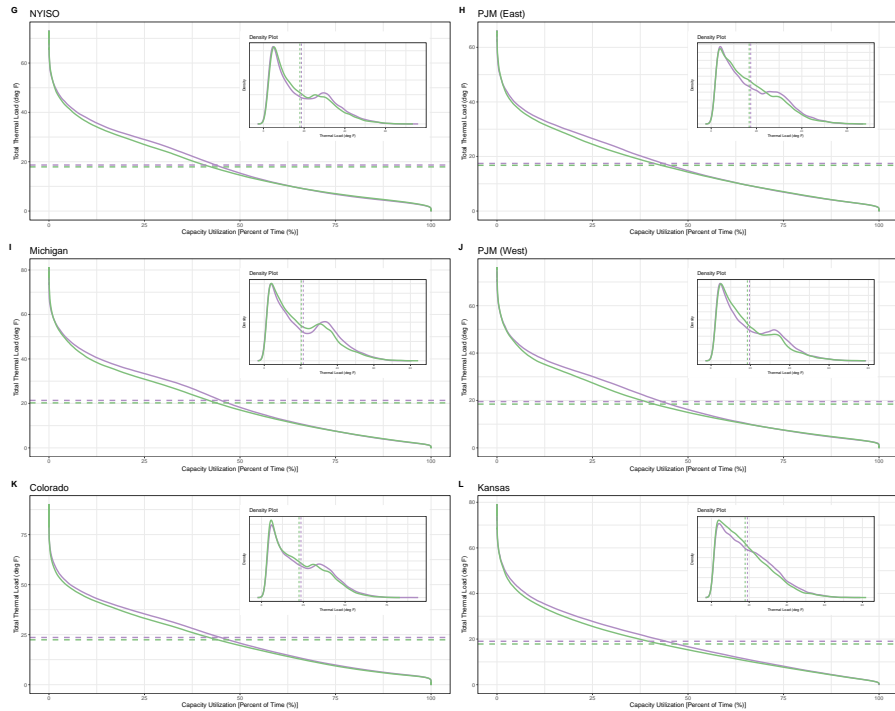


Figure S17: Load duration curves for (G) NYISO, (H) PJM (East), (I) Michigan, (J) PJM (West), (K) Colorado, and (L) Kansas for 1951-1960 (purple line) and 2012-2021 (green line) which correspond to the first and last 10 years of the dataset. The dotted lines denote their respective means. The figure inside the main figure is the probability density function (pdf) of the total thermal load for the two time periods.

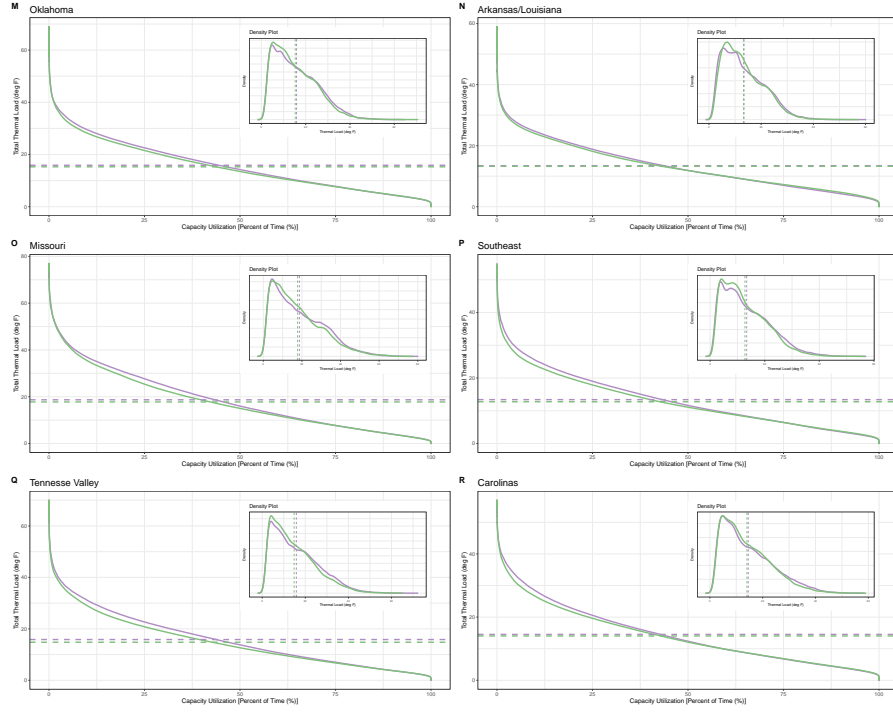


Figure S18: Load duration curves for (M) Oklahoma, (N) Arkansas/Louisiana, (O) Missouri, (P) Southeast, (Q) Tennessee Valley, and (R) Carolinas for 1951-1960 (purple line) and 2012-2021 (green line) which correspond to the first and last 10 years of the dataset. The dotted lines denote their respective means. The figure inside the main figure is the probability density function (pdf) of the total thermal load for the two time periods.

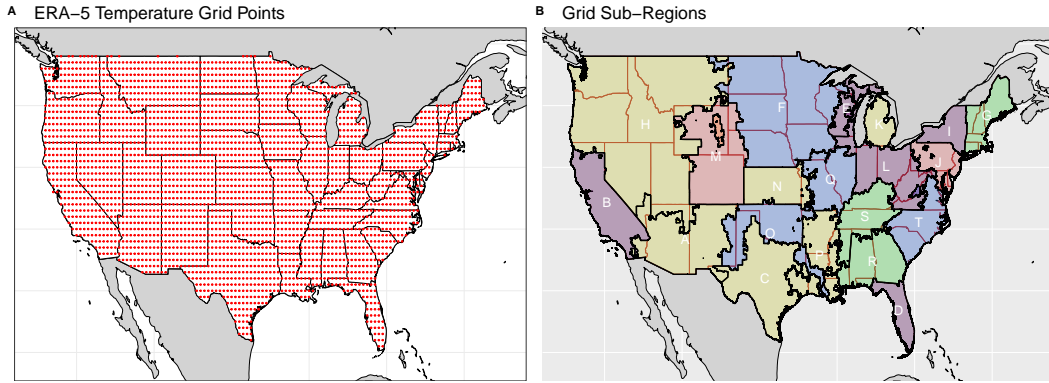


Figure S19: (A) - ERA-5 Temperature grid points across the CONUS. The red dots (3267) are the locations of the grid points (0.5° lat \times 0.5° lon) from the ERA-5 reanalysis dataset. (B) - Grid sub-regions across the CONUS. (A) - Arizona/New Mexico, (B) - CAISO, (C) - ERCOT, (D) - Florida, (E) - Wisconsin (Rural), (F) - Midwest (MISO), (G) - ISO New England, (H) - Northwest, (I) - NYISO, (J) - PJM (West), (K) - Michigan, (L) - PJM (East), (M) - Colorado, (N) - Kansas, (O) - Oklahoma, (P) - Arkansas/Louisiana, (Q) - Missouri, (R) - Southeast, (S) - Tennessee Valley, (T) - Carolinas.